

**Electronic structure and phase stability of MgO, ZnO, CdO, and related ternary alloys**

Y. Z. Zhu, G. D. Chen, and Honggang Ye

*Department of Applied Physics, Xi'an Jiaotong University, Xi'an, Shaanxi 710049, People's Republic of China*

Aron Walsh, C. Y. Moon, and Su-Huai Wei

*National Renewable Energy Laboratory, Golden, Colorado 80401, USA*

(Received 1 April 2008; revised manuscript received 22 May 2008; published 20 June 2008)

The electronic structure and phase stability of MgO, ZnO, CdO, and related alloys in the rocksalt (B1), zincblende (B3), and wurtzite (B4) crystal structures were examined within first-principles band structure theory; the thermodynamically stable phases are reproduced for each material. The band alignment and band-gap deformation potentials were analyzed, showing an increase in the valence band maximum from Mg to Zn to Cd. Ternary alloy formation was explored through application of the special quasirandom structure method. The B1 structure is stable over all (Mg,Cd)O compositions, as expected from the preferences of the binary oxides. The (Mg,Zn)O alloy undergoes a tetrahedral to octahedral transition above 34% Mg content, in agreement with experiment. For (Zn,Cd)O, a transition is predicted above 62% Cd content. These results imply that band-gap manipulation of ZnO from alloying with Mg (Cd) will be limited to 4.0 eV (1.6 eV), while preserving the tetrahedral coordination of the host.

DOI: [10.1103/PhysRevB.77.245209](https://doi.org/10.1103/PhysRevB.77.245209)

PACS number(s): 71.20.Nr, 71.23.An, 71.55.Gs, 78.55.Et

**I. INTRODUCTION**

Demand for greater flexibility in emission wavelengths, increased device performance, and reduced cost is directing the search for new optoelectronic materials away from traditional Al, Ga, and In nitrides, and their solid solutions. Currently, devices composed from the binary oxides of Mg, Zn, Cd, and related alloys are generating considerable interest as they can provide, in principle, an accessible direct band-gap range from around 2.3 eV (539 nm) to 7.7 eV (161 nm). This makes them promising candidates even for deep ultraviolet (UV) lighting applications.<sup>1,2</sup>

Despite the relatively small atomic size mismatch between Mg and Zn, and similar chemical character between Zn and Cd, alloy formation in this system is greatly affected by a segregation outside certain stable compositional ranges.<sup>2</sup> While being formally isovalent, MgO, ZnO, and CdO are not isostructural. The binary oxides of Mg and Cd adopt octahedral coordination in the cubic B1 rocksalt structure ( $Fm\bar{3}m$ ),<sup>3</sup> while Zn favors tetrahedral coordination in the hexagonal B4 wurtzite structure ( $P6_3mc$ ). For ZnO, the cubic B3 zincblende polymorph ( $F\bar{4}3m$ ) lies slightly higher in energy due to its reduced Madelung constant, but the local fourfold coordination environment is similar to wurtzite. Due to this mismatch in coordination preference, alloys formed from Mg, Zn, and Cd exhibit a sensitive structure-composition dependence, with B1, B3, and B4 crystals observed at various alloy compositions and experimental conditions.<sup>2,4,5</sup>

Knowledge of the electronic structure and band alignment of the binary oxides in each crystal structure is therefore of key importance in understanding the alloy properties. Furthermore, due to the forced coupling between the shallow Zn and Cd  $d$  states with O  $2p$  away from  $\Gamma$  in a centrosymmetric  $O_h$  environment, formation of B1 alloys will induce low-intensity indirect transitions unfavorable for optoelectronic applications, so the compositional transition point from tet-

rahedral to octahedral coordination is imperative.

To provide a better understanding of the relationship between the geometric and electronic structure, we have performed first-principles calculations and detailed electronic structure analysis of MgO, ZnO, and CdO in the binary B1, B3, and B4 structures. This includes analysis of the spin-orbit and crystal-field splittings, in addition to the band-gap deformation potentials. Band-alignment calculations show that the valence band (conduction band) rise (fall) on transition from MgO to ZnO to CdO, qualitatively independent of the crystal structure. The properties of the random alloys are also investigated. The B1 phase is found to be stable over all (Mg,Cd)O compositions, as expected from the preferences of the binary oxides. The (Mg,Zn)O alloy is predicted to undergo a tetrahedral to octahedral transition above 34% Mg content, in agreement with experimental data. For the (Zn,Cd)O system, a transition is estimated above 62% Cd content. These results provide a good guideline for the accessible phase space in these alloy systems. Using both the calculated phase transition points and band-gap bowing, we estimate the accessible band-gap range for Zn-rich Cd and Mg tetrahedral alloys as 1.6 to 4.0 eV.

**II. COMPUTATIONAL METHODS**

Calculations were performed using the first-principles density functional theory<sup>6,7</sup> (DFT) based on local density approximation<sup>8</sup> (LDA), as implemented in the relativistic linearized augmented plane wave (LAPW) method.<sup>9,10</sup> The muffin-tin radius of O, Mg, Zn, and Cd were chosen as 1.54, 2.00, 2.00, and 2.40 a.u., respectively. The shallow Zn  $3d$  and Cd  $4d$  states are treated in the same footing as the other  $s$  and  $p$  valence states. The cut-off kinetic energy for the plane wave basis wave functions is 24 Ry. The Monkhorst-Pack<sup>11</sup>  $k$ -point meshes of  $8 \times 8 \times 8$  for the binary structures and equivalent  $k$  points<sup>12</sup> for the superstructures were employed. The bulk structures were each optimized to

their equilibrium volumes through minimization of the total energy. The bulk moduli  $B$  and pressure derivative of the bulk moduli  $B'$  were obtained through a fit of the energy-volume data to the Murnaghan equation of state.<sup>13</sup> The band-gap volume-deformation potentials ( $a_V$ ) were obtained from the relation

$$a_V = \frac{\partial E_g}{\partial \ln V}, \quad (1)$$

while the pressure deformation potentials ( $a_P$ ) were obtained through the application of the bulk modulus:

$$a_P = - \left( \frac{1}{B} \right) a_V. \quad (2)$$

For the determination of the band alignments and alloy formation, only the cubic B1 and B3 structures were explicitly considered, as differences between the direct gap zincblende and wurtzite electronic structures are not large.<sup>14,15</sup> To calculate the “natural” valence band offsets between two binary oxides AO and BO at their respective equilibrium lattice constants, we first calculate the band offsets when the two compounds are in their averaged lattice constant using the approach similar to that used in core level x-ray photoemission spectroscopy,<sup>16,17</sup> that is

$$\Delta E_{v,C'}(\text{AO/BO})_{av} = \Delta E_{v,C'}^{\text{BO}(av)} - \Delta E_{v,C'}^{\text{AO}(av)} + \Delta E_{C,C'}^{\text{AO/BO}(av)}. \quad (3)$$

Here  $\Delta E_{v,C'}^{\text{AO}(av)} = E_{v,C'}^{\text{AO}(av)} - E_C^{\text{AO}(av)}$ , (the same for  $\Delta E_{v,C'}^{\text{BO}(av)}$ ), which is the energy difference between the valence band maximum (VBM) and core level at the average lattice constant.  $\Delta E_{C,C'}^{\text{AO/BO}(av)} = E_{C'}^{\text{BO}(av)} - E_C^{\text{AO}(av)}$  is the energy difference between the two core levels, which can be obtained through a calculation for an unrelaxed  $(\text{AO})_n/(\text{BO})_n$  superlattice at the average lattice constant. In this study, the isostructural band offsets were derived using the  $1s$  core energy levels as references and (001) oriented superlattices. For the B1–B3 offsets, the nonpolar (110)-oriented interface was not chosen due to reported bonding variation at this interface.<sup>18</sup> Instead, a low strain (111) interface was adopted, with an interchange of the anion-cation positions used to average the effects of the dipole. After the band offset is obtained at the averaged lattice constants, the shifts of the VBM states from the averaged lattice constant to equilibrium lattice constant for the binary compounds arising from the VBM absolute deformation potentials<sup>19,20</sup> are included. This approach thus provides a more accurate way to calculate the natural band offsets without making assumptions to the deformation potential of core levels or other reference states.<sup>17</sup>

The random  $\text{A}_{0.5}\text{B}_{0.5}\text{O}$  alloys were modeled within 16-atom (eight mixed cation atom) supercells using the special quasirandom structure (SQS) approach<sup>21,22</sup> to determine the cation site occupancies. These SQS structures (SQS8) are constructed so that the physically most relevant atom-atom correlation functions approach those of random alloys. We assume that the alloys obey Vegard’s law,<sup>23</sup> i.e., the alloy lattice constants are represented by the averaged lattice constants of the constituents. The internal atomic positions inside the SQS cell are fully relaxed through minimization of

TABLE I. Experimental equilibrium structural properties and electronic band gaps (Ref. 24). The internal structural parameter  $u$  for B4 ZnO is 0.382.

|     | Stable Phase | $a$ (Å) | $c/a$ | $E_g^{\Gamma-\Gamma}$ |
|-----|--------------|---------|-------|-----------------------|
| MgO | B1           | 4.216   |       | 7.67                  |
| ZnO | B4           | 3.249   | 1.602 | 3.44                  |
| CdO | B1           | 4.689   |       | 2.28                  |

the quantum mechanical force on each atom to below 0.01 eV/Å. Equivalent  $k$ -point meshes were employed for each SQS structure to ensure good precision when comparing the total energies.<sup>12</sup>

### III. B1, B3, AND B4 BINARIES

#### A. Structural properties

The ground states of MgO, ZnO, and CdO are in the B1, B4, and B1 structures, respectively. The experimental structural parameters<sup>24</sup> are given in Table I. The LDA-calculated B1, B3, and B4 structural parameters, and total energy differences for MgO, ZnO, and CdO are listed in Table II. The calculations reproduce the thermodynamically stable phase of each compound and are in good agreement with experiment and previous theoretical studies.<sup>25,26</sup> The energy difference between the B3 and B4 polymorphs is less than 25 meV per f.u. for ZnO and CdO, and is increased to 75 meV for the highly ionic MgO, with B4 being more stable in each case.

The lattice constants of MgO and ZnO are almost matched. It is interesting to note that in the more ionic B1 structure, MgO is smaller than ZnO, whereas in the more covalent B3 or B4 structure, MgO is larger than ZnO. The lattice constant of CdO is about 10% larger than that of ZnO and MgO. In the B4 structure, the  $c/a$  ratio for ionic MgO and CdO differ significantly from the ideal value of  $\sqrt{8/3} = 1.633$ . To keep the bond lengths similar along and away from the  $c$  direction, the  $u$  parameter should increase when the  $c/a$  parameter decreases (in the ideal case,  $uc/a = \sqrt{3/8}$ ). The bulk moduli are always larger for the B1 structures due to its smaller volume, with the B3 and B4 values almost identical for each compound.

#### B. Band gaps

The calculated band-gap energies are underestimated by the LDA. For B1 MgO, the separation of 4.87 eV between the valence and conduction bands is significantly less than the accepted value of 7.67 eV. In B4 ZnO, the band gap of 0.83 eV relates to the experimental gap of 3.44 eV. For B1 CdO, there is a direct  $\Gamma-\Gamma$  splitting of 1.08 eV, but here the VBM is found along the  $\Gamma-L$  line (due to  $p-d$  coupling away from the zone center), resulting in a negative indirect gap of  $-0.46$  eV (the experimental value is  $\sim 0.84$  eV). Similarly, when placed in the B1 structure, ZnO also exhibits a calculated indirect fundamental gap of 1.12 eV, 1.5 eV less than the direct  $\Gamma-\Gamma$  separation of 2.62 eV.

TABLE II. LDA-calculated equilibrium structural properties and electronic band gaps. For the B4 structure, the internal structural parameters  $u$  are 0.393, 0.380, and 0.389 for MgO, ZnO, and CdO, respectively. The relative total energy ( $\Delta E$  per f.u.) is given with respect to the most stable phase for each compound.

|     | Phase | $a$<br>(Å) | $c/a$ | $\Delta E$<br>(meV) | $B$<br>(Mbar) | $B'$ | $E_g^{\Gamma-\Gamma}$ |
|-----|-------|------------|-------|---------------------|---------------|------|-----------------------|
| MgO | B1    | 4.185      |       | 0                   | 1.74          | 4.24 | 4.87                  |
|     | B3    | 4.556      |       | 384                 | 1.33          | 4.32 | 3.59                  |
|     | B4    | 3.281      | 1.534 | 312                 | 1.32          | 4.34 | 3.48                  |
| ZnO | B1    | 4.224      |       | 185                 | 2.10          | 4.74 | 2.62                  |
|     | B3    | 4.512      |       | 13                  | 1.66          | 4.92 | 0.71                  |
|     | B4    | 3.222      | 1.612 | 0                   | 1.66          | 4.74 | 0.83                  |
| CdO | B1    | 4.650      |       | 0                   | 1.66          | 5.08 | 1.08                  |
|     | B3    | 5.027      |       | 216                 | 1.24          | 5.02 | -0.42                 |
|     | B4    | 3.605      | 1.562 | 191                 | 1.23          | 5.16 | -0.34                 |

Although the LDA calculations severely underestimate the band gap at  $\Gamma$ , the calculated trends are correct. The B1 structures exhibit the largest band gaps at  $\Gamma$  due to the small volume, as well as lack of  $p-d$  repulsion at the  $\Gamma$  point in the  $O_h$  environment. The band gap of the B4 structure is usually larger than the B3 structure due to an increased level repulsion between the valence and the conduction state in the reduced symmetry B4 structure.<sup>27</sup> However, the trend is reversed for MgO. This is because for B4 MgO, the ratio  $c/a=1.534$  is significantly smaller than the ideal value of 1.633, which leads to a large negative crystal field splitting and smaller band gap (see below).

### C. Spin-orbit and crystal-field splittings

For the cubic B1 and B3 structures, the spin-orbit splitting [ $\Delta_0=E(\Gamma_8)-E(\Gamma_7)$ ] can be obtained through a direct comparison of scalar-relativistic and fully relativistic calculations, which splits the sixfold (including spin)  $\Gamma_{15}$  valence band into doubly degenerate  $\Gamma_7$  and fourfold degenerate  $\Gamma_8$  components. However, for the hexagonal B4 structure, there is an additional contribution from crystal field splitting [ $\Delta_{CF}=E(\Gamma_6)-E(\Gamma_1)$ ], which splits the fourfold degenerate  $\Gamma_8$  band into two doubly degenerate  $\Gamma_9$  and  $\Gamma_7$  states. Separation of these effects is possible through the application of the quasicubic model of Hopfield<sup>28</sup>

$$E(\Gamma_9) = \frac{1}{3}(\Delta_0 + \Delta_{CF}),$$

$$E(\Gamma_7^{(1)}) = -\frac{1}{6}(\Delta_0 + \Delta_{CF}) + \frac{1}{2} \left[ (\Delta_0 + \Delta_{CF})^2 - \frac{8}{3}(\Delta_0 \times \Delta_{CF}) \right]^{1/2},$$

$$E(\Gamma_7^{(2)}) = -\frac{1}{6}(\Delta_0 + \Delta_{CF}) - \frac{1}{2} \left[ (\Delta_0 + \Delta_{CF})^2 - \frac{8}{3}(\Delta_0 \times \Delta_{CF}) \right]^{1/2}. \quad (4)$$

The derived spin-orbit (SO) and crystal-field (CF) splittings for all three compounds in each crystal structure are listed in Table III. In the B1 structure, each material exhibits positive spin orbit splittings, increasing from MgO (38 meV) to CdO (68 meV). This is because for the B1 structure, the top of the valence band at  $\Gamma$  has pure O  $p$  and cation  $p$  character. As the cation atomic number increases, the SO splitting increases. In the B3 structure, MgO also exhibits a positive splitting of 34 meV, whereas ZnO and CdO exhibit negative splittings of -39 meV and -54 meV, respectively. The same trend in spin-orbit splittings is observed in the B4 structure. This is because in the tetrahedral environment, the cation  $t_{2d}$  states couple to the O  $p$  states; therefore, for ZnO and CdO in the B3 and B4 structures, the top of the valence band at  $\Gamma$  contains a significant amount of cation  $d$  character. As the  $d$  orbital contributes negative SO splitting, the net SO splittings for ZnO and CdO in the B3 and B4 structures become negative, and the magnitude increases from ZnO to CdO because of the large atomic number of Cd. For MgO, there is no active cation  $d$  orbital, thus, the spin-orbit splitting is still positive. For the CF splitting in the B4 structure, ZnO has a positive CF splitting (101 meV) because the  $\Gamma_{1v}$  state at the top of the valence band is pushed down by the  $\Gamma_1$  conduction band minimum (CBM) state above. However, for CdO the CF splitting (50 meV) becomes smaller and turns to a negative (-334 meV) value for MgO. This arises from the reduced  $c/a$  ratio for CdO and MgO.

Using the calculated SO splitting  $\Delta_0$  and CF splitting  $\Delta_{CF}$  for B4 ZnO and Eq. (4), we find that the order at the VBM of B4 ZnO is  $E(\Gamma_7^{(1)})$ ,  $E(\Gamma_9)$ , and  $E(\Gamma_7^{(2)})$ . This trend is consis-

TABLE III. LDA-calculated spin-orbit ( $\Delta_0$ ) and crystal-field ( $\Delta_{CF}$ ) splittings (meV).

| Splitting     | Phase | MgO  | ZnO | CdO |
|---------------|-------|------|-----|-----|
| $\Delta_0$    | B1    | 38   | 51  | 68  |
| $\Delta_0$    | B3    | 34   | -39 | -54 |
| $\Delta_0$    | B4    | 34   | -41 | -63 |
| $\Delta_{CF}$ | B4    | -334 | 101 | 50  |

TABLE IV. LDA band-gap volume-deformation potentials ( $\alpha_V$ , eV) and pressure coefficients ( $\alpha_P$ , meV/kbar).

|     | Phase | $\alpha_V^{\Gamma-\Gamma}$ | $\alpha_P^{\Gamma-\Gamma}$ | $\alpha_V^{\Gamma-L}$ | $\alpha_P^{\Gamma-L}$ | $\alpha_V^{\Gamma-X}$ | $\alpha_P^{\Gamma-X}$ |
|-----|-------|----------------------------|----------------------------|-----------------------|-----------------------|-----------------------|-----------------------|
| MgO | B1    | -10.08                     | 5.79                       | -6.31                 | 3.63                  | -0.94                 | 0.54                  |
|     | B3    | -5.84                      | 4.39                       | -7.09                 | 5.36                  | -2.29                 | 1.72                  |
|     | B4    | -5.40                      | 4.09                       |                       |                       |                       |                       |
| ZnO | B1    | -9.16                      | 4.37                       | -5.39                 | 2.57                  | -8.52                 | 4.02                  |
|     | B3    | -1.63                      | 0.98                       | -4.05                 | 2.44                  | -0.19                 | 0.11                  |
|     | B4    | -1.72                      | 1.04                       |                       |                       |                       |                       |
| CdO | B1    | -6.35                      | 3.96                       | -4.39                 | 2.73                  | -8.30                 | 5.01                  |
|     | B3    | 0.36                       | -0.29                      | -2.57                 | 2.08                  | -0.60                 | 0.49                  |
|     | B4    | 0.30                       | -0.25                      |                       |                       |                       |                       |

ment with experimental observations.<sup>24</sup> However, because LDA underestimates the band gap and thus overestimates the level repulsion between the CBM  $\Gamma_1$  and the valence band  $\Gamma_{1v}$  state, the calculated CF splitting is too large compared to experimental values ( $\sim 40$  meV). Similarly, due to the underestimation of the Zn *d*-band binding energy, the LDA-calculated SO splitting is too negative compared to the experimental value of about  $-4$  meV. However, the LDA error does not change the sign of  $\Delta_0$  and  $\Delta_{CF}$ , thus the order of the VBM states of B4 ZnO.

#### D. Band-gap deformation

The calculated band-gap pressure and volume-deformation potentials are listed in Table IV. For the B1 phase,  $\alpha_V^{\Gamma-\Gamma}$  is always large and negative, and it becomes less negative on transition from MgO to CdO due to the increase in the anion-cation bond length. For the B3 phase,  $\alpha_V^{\Gamma-\Gamma}$  is negative for both MgO and CdO but becomes positive for CdO; the trend remains the same for the B4 phase. The larger deformation potential of tetrahedral MgO relative to ZnO is consistent with the experimentally observed increase in the pressure coefficient on addition of Mg.<sup>29</sup> The  $\alpha_V^{\Gamma-L}$  and  $\alpha_V^{\Gamma-X}$  potentials remain negative in all cases. However, due to the underestimation of the cation *d* binding energy, the magnitudes of the LDA-calculated band-gap deformation potential are underestimated.

Positive band-gap deformation potentials for the  $\Gamma-\Gamma$  gap are not found in other semiconductor systems,<sup>14</sup> making tetrahedral CdO an anomaly. In general for the valence band, anion *p*-cation *p* coupling results in a strong positive volume-deformation term, which is partially offset by kinetic energy contributions and also by anion *p*-cation *d* coupling when shallow *d* states are present (as for Zn and Cd). The valence *4d* orbitals in CdO are more delocalized; therefore, the *p-d* coupling is more pronounced in CdO than for ZnO, resulting in a small VBM deformation. However, we find that the absolute deformation potential for the VBM of B3 CdO, calculated using the method described in Ref. 20, is still positive (Table V). On the other hand, the conduction-band deformation usually has a strong negative contribution arising from the antibonding anion *s*-cation *s* repulsion and from kinetic energy effects. However, for CdO, we find that

the CBM deformation potential is positive (Table V), which is responsible for the positive band-gap deformation potential. This is because CdO is more ionic. When the compound is compressed, more O *s* character is transferred to the CBM state. As O *s* is more electronegative than Cd *s*, the more attractive potential pulls down the CBM state, resulting to a positive CBM deformation potential. This indicates that in an extremely ionic compound, the covalent tight-bonding band-coupling model does not give a correct description of the deformation potentials.

Our calculated deformation potentials are similar to those calculated by Janotti and Van de Walle<sup>30</sup> using LDA, except that our calculated value for MgO ( $-5.40$  eV) is smaller in magnitude than their LDA value ( $-6.3$  eV). However, our calculated absolute hydrostatic deformation potentials for the individual VBM and CBM states are quite different from their values, possibly because in their calculation no spherical average<sup>19</sup> is performed, i.e., they only calculated epitaxial deformation potentials. Furthermore, they have reported that LDA+*U* calculations give more negative band-gap deformation potentials for B4 ZnO and CdO. However, it is not clear why most of their observed changes occur in the CBM, which is less affected by the Coulomb *U* applied to the occupied cation *d* states.

#### E. Band-edge alignment

The natural band alignment for the valence states are calculated using the procedure described in the previous section

TABLE V. LDA hydrostatic absolute deformation potentials (eV) of the  $\Gamma$  centered VBM (CBM) states of MgO, ZnO, and CdO in the B1 and B3 structures.

|     | Phase | $\alpha_{VBM}$ | $\alpha_{CBM}$ |
|-----|-------|----------------|----------------|
| MgO | B1    | 1.74           | -8.34          |
|     | B3    | 1.66           | -4.18          |
| ZnO | B1    | 2.85           | -6.31          |
|     | B3    | 0.42           | -1.21          |
| CdO | B1    | 3.71           | -2.64          |
|     | B3    | 0.32           | 0.68           |

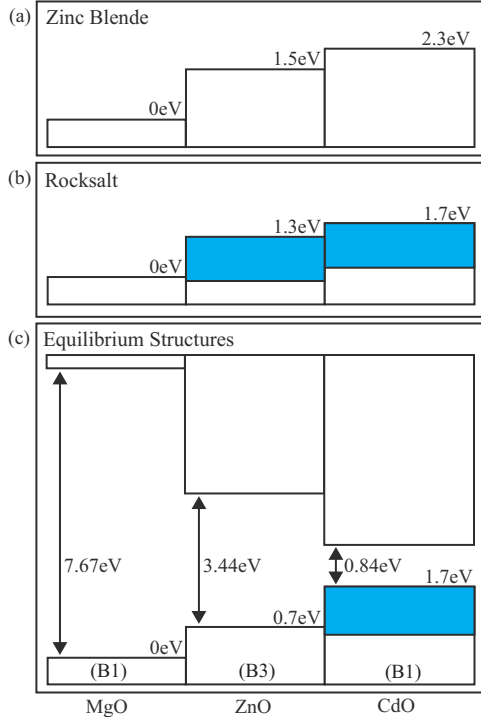


FIG. 1. (Color online) LDA natural band alignments in the (a) B3 and (b) B1 crystal structures. The heterostructural offsets of B1 MgO, B3 ZnO, and B1 CdO are shown in (c). Indirect contributions to the valence band are colored blue (gray).

and the calculated absolute deformation potentials of MgO, ZnO, and CdO in B1 and B3 structures (Table V). The conduction-band offsets are obtained by adding experimental band-gap differences<sup>24</sup> to the calculated valence-band offsets.

The calculated natural band alignments are illustrated in Fig. 1. The B3 isostructural VBMs increase from MgO (0 eV) to ZnO (1.5 eV) to CdO (2.3 eV). This can be understood from the presence of the shallow core  $d$  levels, changes in atomic sizes, and increased covalency of ZnO and CdO relative to MgO.<sup>17</sup> In the B1 phase,  $p$ - $d$  coupling is restricted at  $\Gamma$ , and both the  $\Gamma$ - $\Gamma$  and  $L$ - $\Gamma$  offsets are indicated in Fig. 1. It is clear that both B1 ZnO and CdO contain strong indirect components. The slightly higher VBM of B1 MgO compared to B1 ZnO at  $\Gamma$  is due to the larger bond length of Mg-O compared to Zn-O in this ionic system.

It is also interesting to consider the heterostructural offsets of the stable phases of each compound that takes into account the differences in coordination preference. The offset from B1 MgO to B3 ZnO (0.7 eV) is less than the offset when both are in the B3 structure, indicating that B1 MgO has a higher VBM than B3 MgO. This higher VBM of the octahedral B1 phase compared to the B3 phase of MgO is related to the larger nearest-neighbor separation in the B1 phase and to the fact that the unoccupied Mg  $d$  orbital is above O  $p$ , thus the  $p$ - $d$  coupling pushes down the B3 VBM state of MgO. Recent x-ray photoelectron spectroscopy measurements indicate a type-I alignment for a ZnO/MgO heterojunction, with a valence-band offset of  $0.9 \pm 0.2$  eV.<sup>31</sup> This value is in good agreement with our predictions, but

TABLE VI. Alloy lattice mismatch ( $\Delta a/a$ ), formation energies ( $\Delta H$  per f.u.) and band-gap bowing parameters ( $b$ ).

|          | Phase | $\Delta a/a$<br>% | $\Delta H$<br>(meV) | $b$<br>(eV) |
|----------|-------|-------------------|---------------------|-------------|
| (Mg,Zn)O | B1    | 1                 | 6                   |             |
|          | B3    | 1                 | -18                 | 1.48        |
| (Mg,Cd)O | B1    | 11                | 173                 |             |
|          | B3    | 10                | 4                   | 2.99        |
| (Zn,Cd)O | B1    | 10                | 108                 |             |
|          | B3    | 11                | 35                  | 2.98        |

significantly higher than the calculated offset of 0.24 eV reported by Lany *et al.*<sup>32</sup> from a (112) oriented superlattice.

Our B3 offsets are qualitatively similar to the B4 offsets calculated by Janotti and Van de Walle,<sup>30</sup> but theirs are smaller in magnitude due to a shifting of the cation  $d$  states to higher binding energy within the LDA+ $U$  method.

#### IV. TERNARY ALLOY FORMATION

The three ternary alloys formed from MgO, ZnO, and CdO were investigated in both the B1 and B3 structures at 50%  $A_{0.5}B_{0.5}O$  composition. The resulting structural and electronic properties are listed in Table VI. The formation energy ( $\Delta H$ ) is defined relative to the total energy of the isostructural component phases, i.e.,

$$\Delta H = E(A_{0.5}B_{0.5}O) - \frac{1}{2}[E(AO) + E(BO)]. \quad (5)$$

At 50% composition, (Mg,Zn)O exhibits low formation energies in both alloys, with the B3 phase even becoming slightly negative (-18 meV per f.u.). Such a low barrier to alloy formation arises from the small lattice mismatch (1%) and attractive chemical interactions.<sup>33</sup> Similar negative formation energies have recently been reported for Mg and Zn lithium nitride (I-II-V) alloys.<sup>34,35</sup> The formation energies are higher for both (Mg,Cd)O and (Zn,Cd)O in the B1 phase, but remain low for the B3 phase; the symmetry lowering upon forming the B3 alloy allows for enhanced structural relaxation and Coulomb binding, which compensates for the increased strain.

The band-gap bowing, representing the deviation away from a linear interpolation of the component band gaps, was calculated according to

$$E_g^{\text{Alloy}}(x) = (1-x)(E_g^{\text{AO}}) + x(E_g^{\text{BO}}) - bx(1-x). \quad (6)$$

In this study, we only calculated optical bowing for the direct band-gap B3 alloys. The calculated results are shown in Table VI. We find that the calculated band-gap bowing increases significantly from the low-mismatch (Mg,Zn)O system to the high-mismatch (Mg,Cd)O and (Zn,Cd)O alloys. The bowing coefficients are much larger compared to those of conventional chalcogenide alloys. For example, for the (Zn,Cd)Te alloy, the band-gap bowing parameter is only about 0.3 eV,<sup>21</sup> much smaller than the value of 2.98 eV found

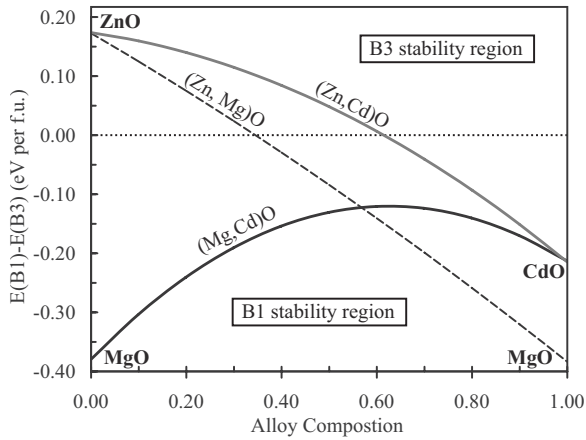


FIG. 2. Energetic stability of the B1 and B3 structures as a function of alloy composition.

for (Zn,Cd)O. This is consistent with the fact that both the lattice mismatch ( $\sim 6\%$ ) and valence band offset ( $\sim 0.3$  eV) in the (Zn,Cd)Te system is smaller than in (Zn,Cd)O.

Similar to the derivation of band-gap bowing, we can estimate the phase stability of each alloy over a wider compositional range from both the total energies of the isolated component phases and the  $A_{0.5}B_{0.5}O$  alloys, i.e.,

$$E_{B1-B3}^{\text{Alloy}}(x) = (1-x)(E_{B1-B3}^{\text{AO}}) + x(E_{B1-B3}^{\text{BO}}) - x(\Omega_{B1-B3})(1-x). \quad (7)$$

The resulting energetic predictions for the B1 and B3 structures [ $E(B1) - E(B3)$ ] are graphed, assuming a compositionally independent interaction energy ( $\Omega$ ), in Fig. 2. For Zn-rich (Mg,Zn)O alloys, tetrahedral coordination in the B3 structure is favored; however, above 34% Mg content a transition to octahedral coordination in the B1 structure is observed. Similarly for (Zn,Cd)O, the B1 structure becomes stable only after the Cd concentration reaches a critical value of 62%. MgO and CdO both favor octahedral coordination and indeed their B1 alloy is predicted to be stable over the entire compositional range.

The results for (Mg,Zn)O are in agreement with both experiment and theory reporting a transition toward the B1

structure above 33% Mg concentration.<sup>5,33</sup> In other theoretical work, only a single alloy phase was considered, so a direct comparison cannot be made.<sup>26,36,37</sup> For (Zn,Cd)O, tetrahedral coordination up to 53% Cd content have been reported.<sup>38</sup>

For optoelectronic applications, the direct band gap provided by the four coordinate structures is most desirable. We can predict the accessible band-gap range of tetrahedral ZnO-based alloys by considering the experimental band gaps of ZnO, CdO (estimated at 1.6 eV for tetrahedral coordination<sup>39</sup>) and MgO (estimated at 6.2 eV for tetrahedral coordination), along with the calculated bowing parameters for the B3 alloys. From Eq. (6), for (Zn,Cd)O and (Mg,Zn)O, the limits of 34% (62%) Mg (Cd) content implies an accessible band-gap range limited to between 1.6 eV to 4.0 eV. For (Zn,Mg)O this threshold has been realized in experiment.<sup>40</sup>

## V. CONCLUSIONS

The detailed electronic structure of MgO, ZnO, CdO, and related alloys has been reported in the B1, B3, and B4 structures at the DFT-LDA level. In each case, the valence (conduction) bands are found to increase (decrease) on transition from Mg to Cd. Both B1 ZnO and CdO are found to contain strongly indirect components. Analysis of the ternary alloys indicates that tetrahedral coordination is only stable in Zn alloys with less than 34% (62%) Mg (Cd) content. This implies that the direct band-gap range will be limited to between 1.6 eV to 4.0 eV before transformation to the B1 structure takes place. However, these limitations may be overcome experimentally through the application of non-equilibrium growth conditions.

## ACKNOWLEDGMENTS

The work at Xi'an Jiaotong University is supported by the National Natural Science Foundation of China under Grant No. 10474078. The work at NREL is supported by the U.S. DOE under Contract No. DE-AC36-99GO10337. Computing resources of the National Energy Research Scientific Computing Center were employed, which is supported by U.S. DOE under Contract No. DE-AC02-05CH11231.

<sup>1</sup>M. Gerhold, A. Osinsky, and D. C. Look, *Quantum Sensing and Nanophotonic Devices III* (SPIE, San Jose, CA, 2006), Vol. 6127, pp. 61271B–12.  
<sup>2</sup>A. Ohtomo, M. Kawasaki, T. Koida, K. Masubuchi, H. Koinuma, Y. Sakurai, Y. Yoshida, T. Yasuda, and Y. Segawa, *Appl. Phys. Lett.* **72**, 2466 (1998).  
<sup>3</sup>D. O. Scanlon, A. Walsh, B. J. Morgan, M. Nolan, J. Fearon, and G. W. Watson, *J. Phys. Chem. C* **111**, 7971 (2007).  
<sup>4</sup>Y.-I. Kim, K. Page, A. M. Limarga, D. R. Clarke, and R. Seshadri, *Phys. Rev. B* **76**, 115204 (2007).  
<sup>5</sup>N. B. Chen and C. H. Sui, *Mater. Sci. Eng., B* **126**, 16 (2006).  
<sup>6</sup>P. Hohenberg and W. Kohn, *Phys. Rev.* **136**, B864 (1964).

<sup>7</sup>W. Kohn and L. J. Sham, *Phys. Rev.* **140**, A1133 (1965).  
<sup>8</sup>D. M. Ceperley and B. J. Alder, *Phys. Rev. Lett.* **45**, 566 (1980).  
<sup>9</sup>S.-H. Wei and H. Krakauer, *Phys. Rev. Lett.* **55**, 1200 (1985).  
<sup>10</sup>D. J. Singh, *Planewaves, Pseudopotentials and the LAPW Method* (Kluwer, Norwell, 1994).  
<sup>11</sup>H. J. Monkhorst and J. D. Pack, *Phys. Rev. B* **13**, 5188 (1976).  
<sup>12</sup>S. Froyen, *Phys. Rev. B* **39**, 3168 (1989).  
<sup>13</sup>F. D. Murnaghan, *Proc. Natl. Acad. Sci. U.S.A.* **30**, 244 (1944).  
<sup>14</sup>S.-H. Wei and A. Zunger, *Phys. Rev. B* **60**, 5404 (1999).  
<sup>15</sup>S.-H. Wei and A. Zunger, *Appl. Phys. Lett.* **69**, 2719 (1996).  
<sup>16</sup>S. P. Kowalczyk, J. T. Cheung, E. A. Kraut, and R. W. Grant, *Phys. Rev. Lett.* **56**, 1605 (1986).

- <sup>17</sup>S.-H. Wei and A. Zunger, Appl. Phys. Lett. **72**, 2011 (1998).
- <sup>18</sup>R. Leitsmann, L. E. Ramos, F. Bechstedt, H. Groiss, F. Schäffler, H. Heiss, K. Koike, H. Harada, and M. Yano, New J. Phys. **8**, 317 (2006).
- <sup>19</sup>Y. H. Li, X. G. Gong, and S.-H. Wei, Phys. Rev. B **73**, 245206 (2006).
- <sup>20</sup>Y. H. Li, X. G. Gong, and S.-H. Wei, Appl. Phys. Lett. **88**, 042104 (2006).
- <sup>21</sup>S.-H. Wei, L. G. Ferreira, J. E. Bernard, and A. Zunger, Phys. Rev. B **42**, 9622 (1990).
- <sup>22</sup>A. Zunger, S.-H. Wei, L. G. Ferreira, and J. E. Bernard, Phys. Rev. Lett. **65**, 353 (1990).
- <sup>23</sup>L. Vegard, Z. Phys. **5**, 17 (1921).
- <sup>24</sup>O. M. Madelung, *Semiconductors: Data Handbook*, 3rd ed. (Springer, Berlin, 2004).
- <sup>25</sup>A. Schleife, F. Fuchs, J. Furthmüller, and F. Bechstedt, Phys. Rev. B **73**, 245212 (2006).
- <sup>26</sup>W. R. L. Lambrecht, S. Limpijumnong, and B. Segall, MRS Internet J. Nitride Semicond. Res. **4S1**, G6.8 (1999).
- <sup>27</sup>G. M. Dalpian, Y. Yan, and S.-H. Wei, Appl. Phys. Lett. **89**, 011907 (2006).
- <sup>28</sup>J. J. Hopfield, J. Phys. Chem. Solids **15**, 97 (1960).
- <sup>29</sup>J. Huso, J. L. Morrison, H. Hoock, X.-B. Chen, L. Bergman, S. J. Jokela, M. D. McCluskey, and T. Zheleva, Appl. Phys. Lett. **89**, 171909 (2006).
- <sup>30</sup>A. Janotti and C. G. Van de Walle, Phys. Rev. B **75**, 121201(R) (2007).
- <sup>31</sup>Y. F. Li *et al.*, Appl. Phys. Lett. **92**, 192116 (2008).
- <sup>32</sup>S. Lany, J. Osorio-Guillén, and A. Zunger, Phys. Rev. B **75**, 241203(R) (2007).
- <sup>33</sup>M. Sanati, G. L. W. Hart, and A. Zunger, Phys. Rev. B **68**, 155210 (2003).
- <sup>34</sup>A. Walsh and S.-H. Wei, Phys. Rev. B **76**, 195208 (2007).
- <sup>35</sup>A. Walsh and S.-H. Wei, Phys. Status Solidi C **5**, 2326 (2008).
- <sup>36</sup>B. Amrani, R. Ahmed, and F. El Haj Hassan, Comput. Mater. Sci. **40**, 66 (2007).
- <sup>37</sup>H. Rozale, B. Bouhafs, and P. Ruterana, Superlattices Microstruct. **42**, 165 (2007).
- <sup>38</sup>D. W. Ma, Z. Z. Ye, and Y. S. Yang, Appl. Phys. B: Lasers Opt. **82**, 85 (2006).
- <sup>39</sup>C. Y. Moon, S.-H. Wei, Y. Z. Zhu, and G. D. Chen, Phys. Rev. B **74**, 233202 (2006).
- <sup>40</sup>A. K. Sharma, J. Narayan, J. F. Muth, C. W. Teng, C. Jin, A. Kvit, R. M. Kolbas, and O. W. Holland, Appl. Phys. Lett. **75**, 3327 (1999).